NeuroImage 211 (2020) 116597

Contents lists available at ScienceDirect

NeuroImage

journal homepage: www.elsevier.com/locate/neuroimage

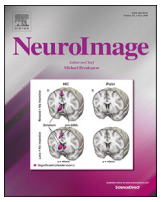

Cortical hemodynamic responses induced by low-intensity transcranial ultrasound stimulation of mouse cortex

Yi Yuan [a,b,*,1], Zhijie Wang [a,1], Mengyang Liu [c], Shy Shoham [b,**]

[a] Institute of Electrical Engineering, Yanshan University, Qinhuangdao, 066004, China
[b] Departments of Ophthalmology, Departments of Neuroscience and Physiology, NYU Langone Health, New York, 10016, USA
[c] Center for Medical Physics and Biomedical Engineering, Medical University of Vienna, Vienna, 1090, Austria

ARTICLE INFO

Keywords:
Transcranial ultrasound stimulation
Motor response
Neural activity
Hemodynamic
LSCI
Multi-parameter

ABSTRACT

Ultrasound-mediated neuromodulation is emerging as a key technology for targeted noninvasive brain stimulation, but key insights into its effects and dose-response characteristics are still missing. The purpose of this study is to systematically evaluate the effect of low-intensity transcranial ultrasound stimulation (TUS) on complementary aspects of cerebral hemodynamic. We simultaneously record the EMG signal, local field potential (LFP) and cortical blood flow (CBF) using electrophysiological recording and laser speckle contrast imaging under ultrasound stimulation to simultaneously monitor motor responses, neural activities and hemodynamic changes during the application of low-intensity TUS in mouse motor cortex, using excitation pulses which caused whisker and tail movement. Our experimental results demonstrate interdependent TUS-induced motor, neural activity and hemodynamic responses that peak approximately 0.55s, 1.05s and 2.5s after TUS onset, respectively, and show a linear coupling relationship between their respective varying response amplitudes to repeated stimuli. We also found monotonic dose-response parametric relations of the CBF peak value increase as a function of stimulation intensity and duration, while stimulus duty-cycle had only a weak effect on peak responses. These findings demonstrate that TUS induces a change in cortical hemodynamics and LSCI provide a high temporal resolution view of these changes.

1. Introduction

As a close proxy to cortical activity, cerebral hemodynamics studies are important for characterizing, validating and optimizing the effects induced by brain neuromodulation, and for illuminating and studying the underlying modulation mechanisms (Koch et al., 2009; Thomson et al., 2011). Indeed, studies utilizing neuroimaging techniques such as functional magnetic resonance imaging, near-infrared spectroscopy or positron emission computed tomography found that deep brain stimulation (Shih et al., 2014), transcranial direct current stimulation (Baudewig et al., 2001) and transcranial magnetic stimulation (Hubl et al., 2008) systematically alter cerebral hemodynamics.

Low-intensity transcranial ultrasound stimulation (TUS) is emerging as a new modality for noninvasive neuromodulation (Naor et al., 2016), with advantageous characteristics of high spatial resolution and penetration depth in comparison to transcranial direct current stimulation and transcranial magnetic stimulation. Multiple earlier studies have demonstrated that TUS can causally modulate brain activity, including the induction of motor responses (King et al., 2013; Yu et al., 2016; Yuan et al., 2016). However, to date only a few scattered studies examined the effect of TUS on cerebral hemodynamics. Yoo et al. (2011) used functional magnetic resonance imaging to monitor blood-oxygen level-dependent signals induced by TUS in rabbits, finding signal responses on the order of 1.5% at acoustic intensities $\geq$3.3 W/cm^2. However, due to the technique's limitations, this foundational study did not map the fine temporal properties of the hemodynamic TUS-responses. In recent work, Kim et al. (2017) monitored cerebral hemodynamic changes during TUS by intrinsic signal optical imaging in mice, showing that ultrasonic stimulation increases hemoglobin oxygenation and that the response amplitude is related to the pulse repetition frequency. However, their protocol used a very low (non-standard) ~7% duty cycle which likely elicited mixed suppression-excitation responses and was not shown to elicit any

* Corresponding author. Institute of Electrical Engineering, Yanshan University, Qinhuangdao, 066004, China.
** Corresponding author.
E-mail addresses: yuanyi513@163.com (Y. Yuan), shoham@nyu.edu (S. Shoham).
[1] These authors have contributed equally to this work.

https://doi.org/10.1016/j.neuroimage.2020.116597
Received 7 November 2019; Received in revised form 28 December 2019; Accepted 31 January 2020
Available online 1 February 2020

causal motor responses or other localized responses (Kim et al., 2017; Plaksin et al., 2014). Moreover, their 5-s-long cortical ultrasound stimulation protocol continuously extends over most of the response duration, and thus precludes observing a unitary hemodynamic response function to single short TUS pulses, and its precise onset and return times and response duration remain unknown.

Another well-known aspect of ultrasound neuromodulation is the key role that ultrasound parameters play in leading to different stimulation effects, including a transition between stimulation and suppression regimes (Yoo et al., 2011; Plaksin et al., 2016). To characterize parameter dependence, King et al. (2013) used TUS to stimulate the mouse nervous system *in vivo* and to induce motor responses. They found that stimulation success systematically increases as a function of both ultrasonic intensity (UI) and stimulation duration (SD). Kim et al. (2014) examined the range of ultrasonic parameters that minimize the UI while successfully stimulating the motor brain area in Sprague-Dawley rats. They also found that motor responses were related to UI. However, the temporal cerebral hemodynamic response characteristics with different stimulus parameters including UI, SD and duty cycle (DC) remain unclear.

Here, we aim to address a gap left open by these earlier studies, by using laser speckle LSCI in mice to measure at high temporal resolution the cortical hemodynamic responses induced by a relatively standard, short TUS protocol that is shown to elicit causal motor responses and neural activity. Hemodynamic responses induced by multi-parameter ultrasound were analyzed in a cohort of mice. We find that relatively rapid hemodynamic responses follow the motor responses to single-pulse TUS, and that there is the linear coupling relationship between the hemodynamic, motor response and neural activity. Furthermore, the peak values of CBF increase as increase of ultrasonic intensity and stimulation duration. These findings inform our interpretation of short-term stimuli driven immediate hemodynamic response, and provide a quantitative investigation of hemodynamic response in TUS with multi-parameter.

2. Materials and methods

2.1. Animal surgery and anesthesia

A total of twenty-nine BALB/c mice were used in the experiments (all male, body weights 20–25g, ages 4–5 weeks, Beijing Vital River Laboratory Animal Technology Co., Ltd. China; nine mice were used for ISOI and twenty mice for LSCI). All procedures were carried out according to the Animal Ethics and Administrative Council of Yanshan University. Furthermore, the manuscript was written in accordance with the ARRIVE (Animal Research: Reporting In Vivo Experiments) guidelines. Surgical anesthesia was induced with sodium pentobarbital (3%, 5 mg/100g, i.p.), and lasted throughout the stimulation experiments. The anesthetized mice were fixed on a stereotaxic apparatus (ST-5ND-C, Stoelting Co., U.S.A) with ear bars and a clamping device. The surgical procedure is similar to our previous study (Yuan et al., 2019). A 4 mm × 4 mm square skull section was removed to expose the brain tissue. The mice's body temperature was maintained at 37 °C using a closed-loop animal temperature controller (69002, RWD., Shenzhen, China).

2.2. Experimental groups and US parameters

Three groups were used in our experiments: Group 1, six mice for the tail motor response, neural activity and CBF response experiments. Group 2, nine mice for the whisker motor response and deoxyhemoglobin metabolism. Group 3, eleven mice for CBF response vs multi-parameters. Group 4, three mice for evaluating the thermal effects for CBF response. An f = 500 kHz US frequency, 1 kHz PRF pulse train was used across all experiments. For group 1 and group 2, the SD and DC were 400 ms and 40%, respectively. For the group 3, additional combinations of ultrasound parameters were used, including I_{sppa}, DC and SD as shown in Table 1. The sequence diagram of the ultrasound stimulation and image recording is shown in Fig. 1(C).

Table 1
Combination of ultrasonic parameters used in this study (FF = 500 kHz, PRF = 1 kHz).

I_{sppa}(W/cm^2), SD = 400 ms, DC = 40%	SD(ms), I_{sppa} = 0.8 W/cm^2, DC = 40%	DC(%), I_{sppa} = 0.8 W/cm^2, SD = 400 ms
0.2	50	10
0.4	100	20
0.8	200	30
1.1	300	40
	400	

2.3. Combined TUS - optical imaging experimental setup

The schematic of the experimental setup is shown in Fig. 1(A). The TUS setup is similar to the setup used in our previous study (Yuan et al., 2019). An unfocused ultrasound transducer (V301-SU, Olympus, USA) with center frequency f = 500 kHz and a 31 mm diameter. A 3D-manual adjustment is used to fix the transducer so that it can accurately move to the stimulus position. The ultrasound transducer connects to the mouse skull by a 3D printed conical coupling cone that is filled with an ultrasound coupling gel. The gap between the coupling cone and skull is filled with glycerol so that the ultrasound wave can stimulate the brain tissue. The two-dimensional distribution of ultrasound field in oblique and longitudinal cross section (Fig. 1(B)) is measured by a calibrated needle-type hydrophone (HNR500, Onda, Sunnyvale, CA).

2.4. Optical imaging experimental setup

A custom imaging system was configured to perform LSCI. The system is based on a monocular tube microscope (CM-10, Nikon, Japan) with an extended working-distance objective lens (Working distance: 34.6 mm, NA: 0.055, WD-5002, PDV, China). A CCD camera (Pixelfly, 14bit, PCO, Germany) mounted on the single-passed microscope is used to record the raw images. An electronic lifting platform (KSAV1010-ZF, Zolix, China) placed under the mouse stereotaxic apparatus was used to adjust the distance between the objective lens and the mouse's head, for image focusing. A diode laser (MW-SGX-635, 635 nm, 20 mW, Leishi, China) beam coupled with a 600-nm diameter silica optical fiber is used as the light source. The laser speckle images were acquired at 21fps (frame per second) and the exposure time was 20 ms.

2.5. LSCI image reconstruction

The speckle contrast value (K) is calculated as the ratio of standard deviation (σ_s) to the mean intensity of each binning window <I>. The raw images recorded by the camera are converted to speckle contrast images using Eq. (3).

$$K = \frac{\sigma_S}{\langle I \rangle} = \left\{ \frac{\tau_C}{2T} \left[1 - \exp\left(-\frac{2T}{\tau_C} \right) \right] \right\}^{0.5} \tag{3}$$

where T is exposure time of the camera, τ_c is the correlation time, which is assumed to be inversely proportional to a measure of the velocity of the scattering particles. In our study, temporal laser speckle contrast analysis algorithm was used to calculate the contrast value from the speckle images (Li et al., 2009).

2.6. LFP and EMG recording

A tungsten microelectrode (WE50030.1B10, MicroProbe, USA) and a homemade EMG electrode (Tufail et al., 2011) were used for recording LFP signal and EMG signal, respectively. The LFP signals and EMG signals were simultaneously recorded by using a dual-channel pre-amplifier (63386, A-M Systems Inc., USA) and saved by a neural signal processor system. (Cerebus Data Acquisition System, Blackrock Microsystems, USA). The raw LFP signals and EMG signals produced in response to TUS

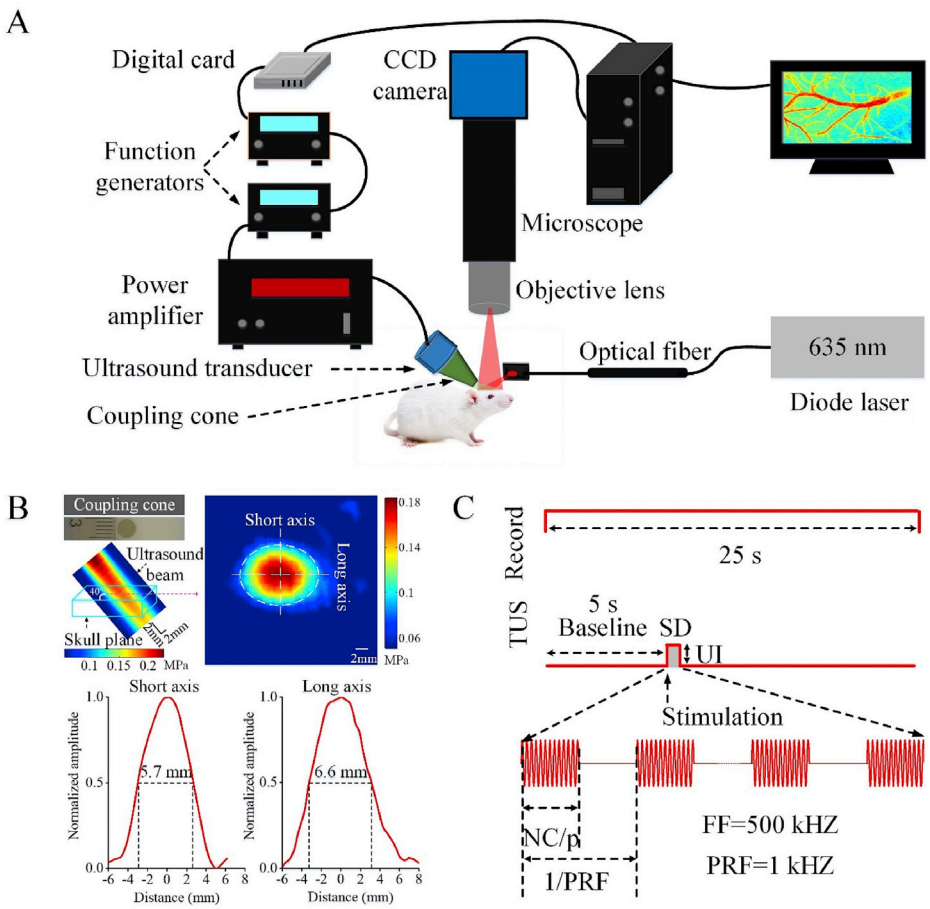

Fig. 1. Experimental setup and protocol. (A) Schematic of ultrasound stimulation and optical imaging system. The transducer connects to the mouse head by a coupling cone filled with ultrasound coupling gel. There is a thin layer of glycerin between the coupling cone and the skull. The angle between the coupling cone and the skull is about 40°. A microscope directly above the mouse head records raw optical images. Light of brain. For LSCI, the light wavelength is 635 nm, irradiates the imaging region from the side. (B) The 2D distribution of the ultrasound field in oblique and longitudinal cross section. The long axis and short axis of ultrasound spot is ~6.5 mm and ~5.7 mm, respectively. (C) Time sequence of the imaging experiments in which a CCD camera records for 25s. Ultrasound was delivered to brain tissue followed by baseline of 5s. Sixteen trials were averaged to improve signal-to-noise ratio. TBD: tone burst duration, FF: fundamental frequency, NC/p: number of cycles per pulse, UI: ultrasonic intensity, SD: stimulation duration, PRF: pulse repetition frequency.

were acquired at a sampling frequency of 2 kHz.

2.7. Analysis of LFP signals and EMG signals

We analyzed the amplitude of EMG and LFP signals. The EMG waveform was obtained from raw EMG signals by FIR filtering from 300 to 1000Hz according to the literature (King et al., 2013). The mean amplitude (MAMP) of the signals before and after TUS were calculated by the formula

$$MAMP = \sum_{T_1}^{T_2} |AMP| \Big/ (T_2 - T_1) \quad (1)$$

where AMP is the amplitude of signal, and T_1 and T_2 are the start and end time of the signal. The percent change in the MAMP was calculated using the following formula:

$$\Delta MAMP / MAMP = (MAMP_{t1-t2} - MAMP_{-3-0s}) / MAMP_{-3-0s} \quad (2)$$

where $MAMP_{t1\text{-}t2}$ is the mean amplitude between time t_1 and time t_2, the interval is 0.1s. $MAMP_{-3\text{-}0}$ is the mean amplitude between from -3s to 0s and used for baseline. We defined 0s as the starting point of the TUS.

2.8. Data statistics

All data processing procedures were implemented in MATLAB (Mathworks, Natick, Massachusetts, USA). In data analysis, we take the time of stimulus onset as the zero moment. The statistics method is Friedman test in our study.

3. Results

3.1. Motor response induced by low-intensity TUS

First, to verify that our TUS protocol induces time-locked neural excitation, we monitored bilateral whisker and tail motion during the stimulation paradigm. As shown in Fig. 2 (A), the mouse whiskers move bilaterally during TUS, with their orientation displaced relative to the pre-stim observed orientation. Whisker motion continues until relaxing back to their rest orientation. The entire stimulus-response dynamical process is shown in Fig. 2(A), where the abrupt and overt bilateral whiskers' response to TUS is clearly visible. We consistently observed these bilateral whisker motor responses in all the mice used in our experiments. Measuring the central whisker's distances relative to rest (Fig. 2(B)) indicates that the maximum displacement is observed approximately at t = 0.1s, while the complete relaxation back to baseline process lasts to ~1s. As shown in Fig. 2(C), the mouse tail moves during TUS and the tail motion continues until relaxing back to their rest orientation as shown in video in the supplementary material. Fig. 2(D) is the trigger signal of TUS, EMG signal (300–1000Hz) and LFP signal (4–500Hz) (from one representative mouse) indicate that there is the immediate motor response and neural activity with TUS. These results confirm that our stimulation protocol modulates neuronal activity, triggering a robust bilateral whisker and tail motor response.

3.2. Characteristics and coupling of TUS-induced neuro-vascular responses

We next studied the fundamental characteristics of the TUS-induced time-locked neural activity and hemodynamic responses, by simultaneously monitoring LFP and CBF signals in addition to the motor-related

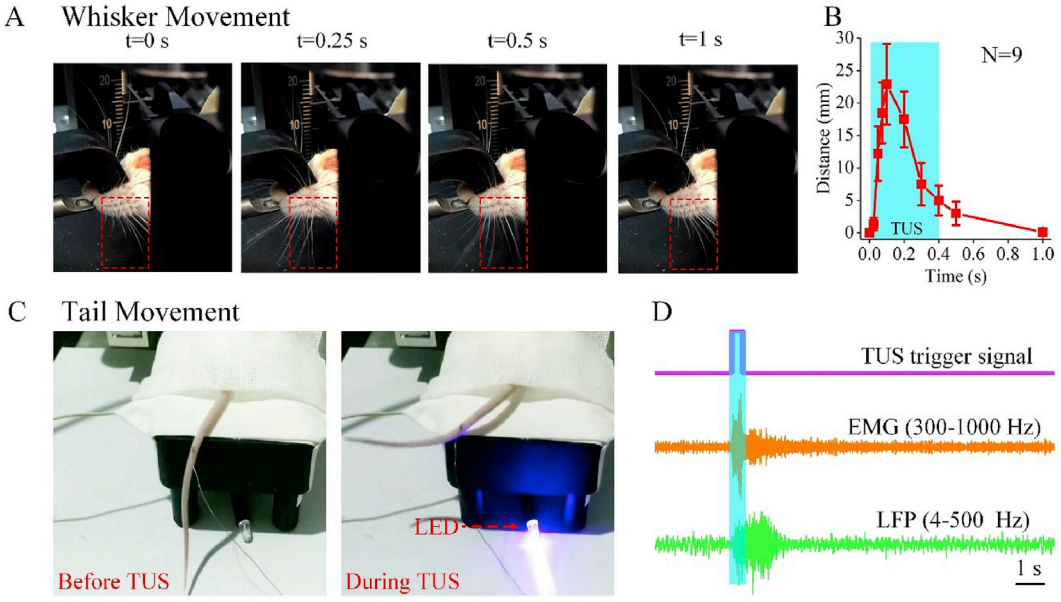

Fig. 2. Motor response. (A) Whisker movement: time-lapse photographs of representative mouse bilateral whisker field immediately before, during and after the ultrasonic stimulus onset (t = 0). (B) The displacement of one whisker at different times relative to TUS (N = 9). (C) Tail movement: Motor response of mouse tail before and during the TUS. (D) The trigger signal of TUS and the corresponding EMG signal (300–1000Hz) and LFP signal (4–500Hz) for one trial.

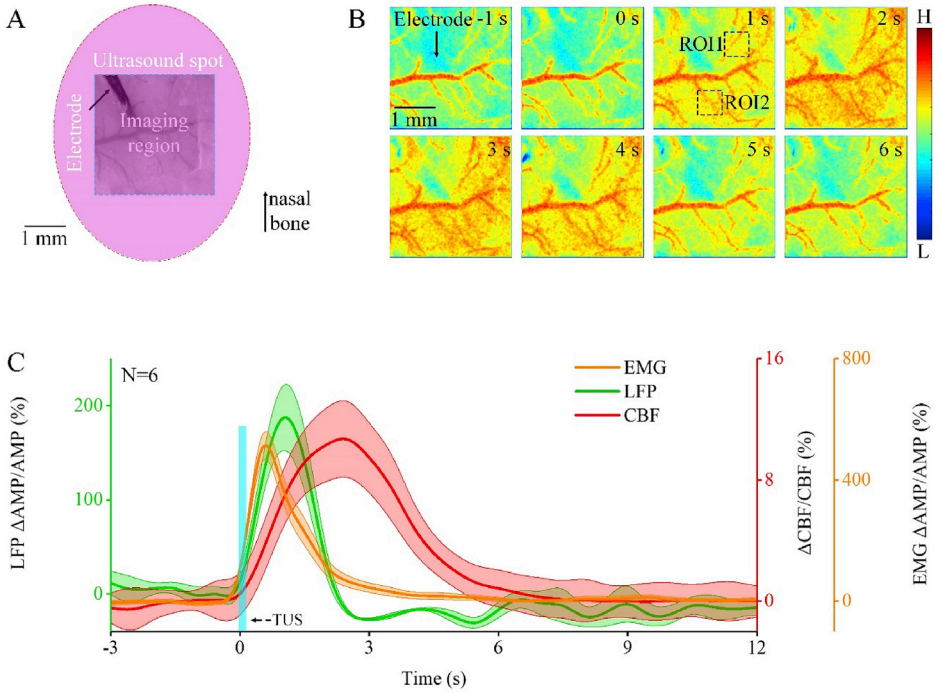

Fig. 3. TUS-induced time-locked neural activity and hemodynamic responses. (A) Location of ultrasound spot and electrode in motor cortex. (B) The raw CBF image of CBF response induced by TUS in one mouse (average values with 16 trials). (C) The EMG, LFP and CBF response induced by TUS (N = 6, Mean ± SEM) (I_{sppa} = 1.1 W/cm^2, SD = 400 ms, DC = 40%).

EMG signals during the stimulation paradigm. Fig. 3(B) shows the temporal evolution of a representative CBF response induced by TUS, (I_{sppa} = 1.1 W/cm^2, SD = 400 ms, DC = 40%). Comparing to the baseline image at t = -1s, we observe a CBF response that begins as early as 1s, peaks and then decreases gradually back to baseline at t ~ 5s. The different motor, LFP and CBF average response time traces (Fig. 3(C), N = 6, Mean ± SEM), clearly demonstrate the TUS-evoked impulse response functions that peak at ~0.55s, ~1.05s, ~2.5s and decay back to baseline by ~3.7s, ~2.6s and ~5.5s, respectively. These experimental results show that TUS induces motor, neural and hemodynamic responses, putatively by stimulating motor cortex.

To further study and potentially establish this putative relationship we next examined several related aspects and potential confounds of these observed responses. First, we examined whether our TUS protocol also induces changes in the brain's blood oxygen metabolism, by measuring the associated HbR responses (Fig. S1; N = 9, Mean ± SEM).

The results indicate that in response to TUS ΔR/R increases to a peak value, reached 2.55 ± 0.09s after the stimulation was initiated, and then decreases gradually until t ~ 6s (reaching a weak overshoot of the baseline value), demonstrating that the TUS-induced systematic HbR change in brain tissue, quite closely mirrors the CBF response. We next examined the possibility that the observed CBF responses are directly thermally-induced. Previous studies have shown that when ultrasound acts on brain tissue, the thermal effect (temperature rise) produced can directly cause CBF increase (Hynynen et al., 1997; Vykhodtseva et al., 2000; Constans et al., 2018). In order to examine a possible direct causality between the CBF changes and thermal effect, we performed additional experiments in three mice under the maximum ultrasound parameters (I_{sppa} = 1.1 W/cm^2, SD = 400 ms, DC = 40%) with 2% isoflurane. The results (Fig. S2) show no significant motor, neural activity (LFP) or hemodynamic CBF changes consistent with the results of earlier studies on lack of ultrasound neuromodulation effects under deep aesthesia (1.8–2% isoflurane) (King et al., 2013; Younan et al., 2013; Kim et al., 2017). These results also discount the possibility that the CBF change is caused directly by the thermal effect. Indeed, our expected TUS-induced temperature change is approx. ~4.8 × 10^{-3} °C, also suggesting that this effect should be minimal (calculated using: $\Delta T = \frac{2\alpha It}{\rho_b C_p}$ (Lee et al., 2015), where α is the absorption coefficient and equals 0.0175 cm^{-1}, ρ_b is the density of brain tissue, C_p is the specific heat of brain tissue, and the product $\rho_b C_p$ is equal to 3.811J cm^3 °C^{-1}. the ultrasound intensity I is equal 1.1 W/cm^2 and pulse duration t is 0.05s. Finally, to further understand the relations between the neural and vascular responses. We analyzed the coupling between the motor response, neural activity and hemodynamic response. Fig. 4(A) is the curve of ΔCBF/CBF in ROIs from Fig. 3(B) for each trail and Fig. 4(B) shows the mean curve of ΔCBF/CBF for sixteen trials. The coupling of CBF vs. LFP, EMG vs. LFP and EMG vs. CBF for each mouse was shown in Figs. S1–S3. The Coupling between CBF, LFP and EMG for 16 trials across all animals were shown in Fig. 4(C)–(E). The results demonstrate that there is the linear coupling relationship between the CBF, LFP and EMG.

3.3. CBF response dependence on ultrasound parameters

Finally, we quantitatively evaluated in a group of eleven mice the effect on observed CBF responses of varying three ultrasonic excitation parameters: intensity (I_{sppa}), duration (SD) and duty cycle (DC). We observed monotonically increasing ΔCBF/CBF responses with increasing intensities (Fig. 5(A1), I_{sppa} range: 0.2–1.1 W/cm^2; SD = 400 ms, DC = 40%). Peak ΔCBF/CBF values were 5.3 ± 1.9%, 7.9 ± 2.2%, 10.4 ± 2.1% and 13.4 ± 1.9% for I_{sppa} = {0.2, 0.4, 0.8, 1.1} (W/cm^2), respectively (Fig. 5 (A2), Mean ± SEM, N = 11; results indicate significant differences using Friedman test, *p < 0.05). As shown in Fig. 5(B1), CBF peak responses also increase monotonically with increasing SD (I_{sppa} = 0.8 W/cm^2, DC = 40%). The peak ΔCBF/CBF values were 5.6 ± 1.6%, 6.9 ± 1.7%, 8.9 ± 1.9%, 10 ± 1.9%, 10.4 ± 2.1% for SD = {50, 100, 200, 300, 400}ms, respectively, (Fig. 5(B2), Mean ± SEM, Friedman test, *p < 0.05). The results indicated that the peak ΔCBF/CBF response values increase as increasing SD.In contrast to the previous parameter dependences, the ΔCBF/CBF responses had a relatively weak dependence on DC (Fig. 5(C1), I_{sppa} = 0.8 W/cm^2, SD = 400 ms). The mean peak ΔCBF/CBF values were 9.0 ± 2.0%, 9.5 ± 2.0%, 11.2 ± 2.3% and 10.4 ± 2.1% for DC = {10%, 20%, 30%, 40%}, respectively, (Fig. 5 (C2), Mean ± SEM, N = 11, Friedman test, p > 0.05).

4. Discussion

In this study, we used low-intensity TUS to stimulate mouse motor cortical regions and simultaneously recorded the EMG signals, LFP signals and laser speckle contrast images. We successfully and robustly elicited tail movement, neural activity and CBF response, in agreement

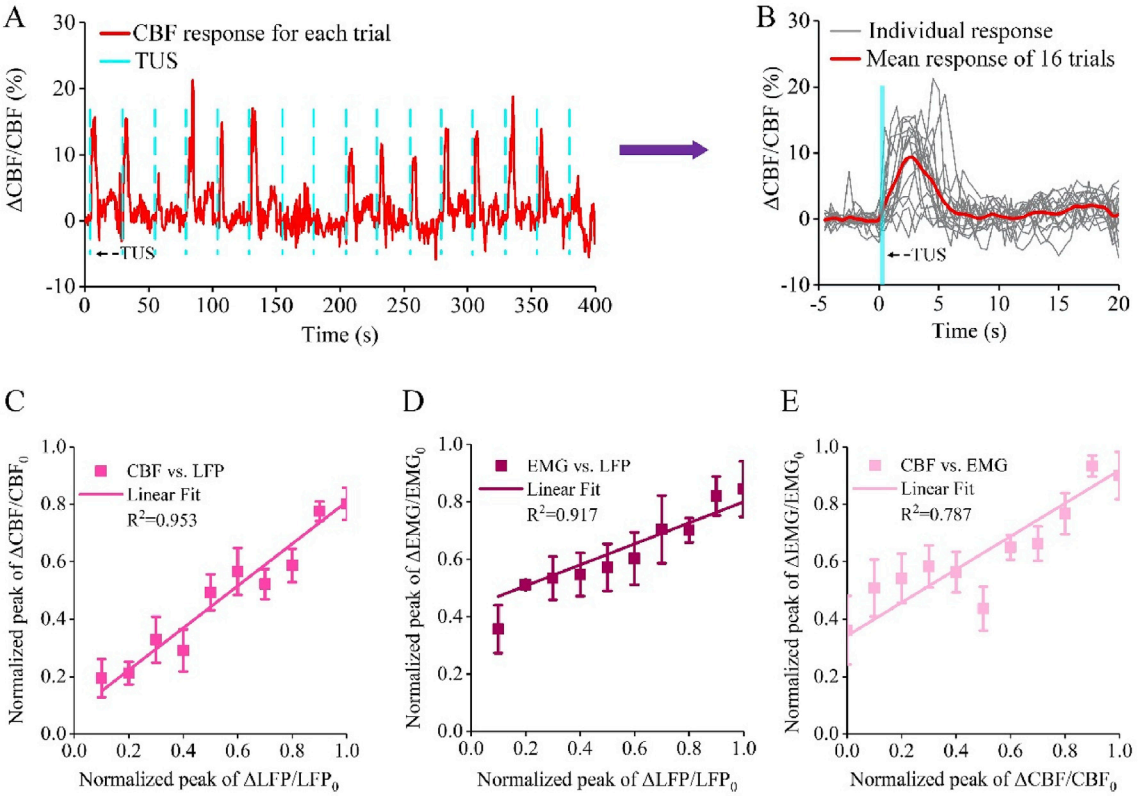

Fig. 4. Coupling of TUS-induced neuro-vascular responses. (A) The curve of CBF response (ΔCBF/CBF) induced by TUS from ROIs in Fig. 2(B) for 16 trials. (B) The average values of 16 trials from Fig. 3 (A). (C)–(E) Fig. 4. Coupling between CBF, LFP and EMG for 16 trials across all animals, (C) CBF vs. LFP, (D) EMG vs. LFP, (E) CBF vs. EMG. (N = 6, Mean ± SEM) (I_{sppa} = 1.1 W/cm^2, SD = 400 ms, DC = 40%).

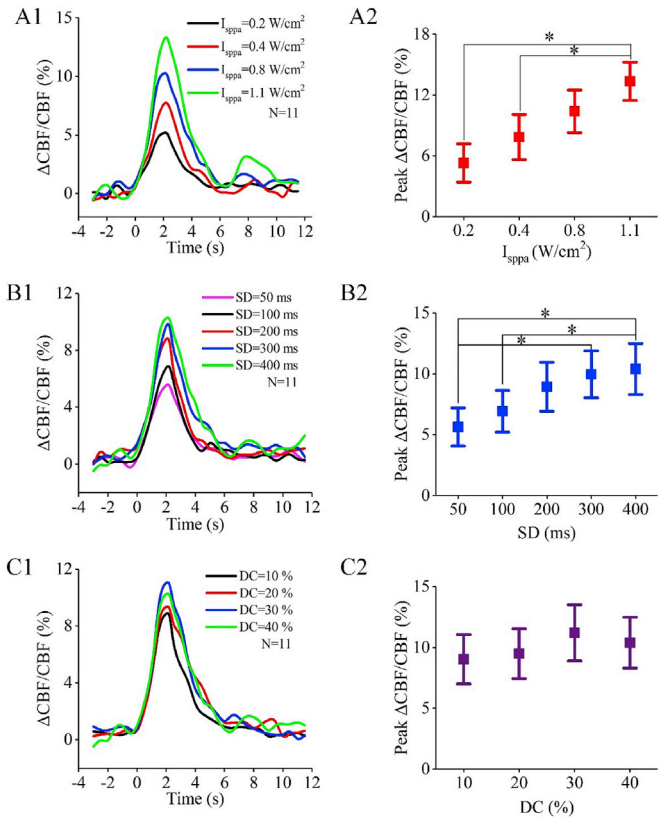

Fig. 5. CBF responses to varying US parameters (I_{sppa}, SD and DC; N = 11 animals). (A1) CBF responses to different I_{sppa} values (fixed parameters: SD = 400 ms, DC = 40%). (A2) Statistical results (Mean ± SEM, Friedman test, *p < 0.05). (B1) CBF response functions for different SD (I_{sppa} = 0.8 W/cm^2, DC = 40%). (B2) Statistical comparisons for peak ΔCBF/CBF values (Mean ± SEM, Friedman test, *p < 0.05). (C1) CBF responses for different duty cycles (I_{sppa} = 0.8 W/cm^2, SD = 400 ms). (C2) Statistical comparisons for peak values of ΔCBF/CBF.

with the results of earlier studies (Younan et al., 2013). We observed the immediate movement and neural activity responses that peaked 0.55s and 1.05s after the stimulation and returned to baseline at ~3.7s and ~2.6s, respectively. We also observed relatively rapid CBF responses that peaked 2.5 ± 0.1s after the stimulation and returned to baseline at ~5.5s. Our study also includes a multi-parameter characterization of the CBF responses to TUS stimulation of mouse motor cortex, which, to our knowledge, is the first study on the relationships between CBF and key ultrasound parameters. Our results indicate that the CBF responses are strongly modulated by intensity and stimulus duration while only being weakly affected by the pulse duty cycle (the detailed dependence is further discussed below).

How does the observed hemodynamic response function compare to earlier observations? Our estimates generally have noticeably faster dynamics than others. For example, the fMRI BOLD hemodynamic response induced by ultrasound stimulation in Yoo et al. (2011) reached a maximum value at ~3.2s after ultrasound stimulus onset for both 3.3 and 6.4 W/cm^2 I_{sppa} (PRF = 10Hz, SD = 1s, DC = 50%). However, these observations were in rabbits, and were also obtained with a long excitation pulse and at a relatively low temporal resolution. Yang et al. (2018) used fMRI to monitor ultrasound neuromodulation of sensory networks in the monkey brain (f = 250 kHz, PRF = 2 kHz, I_{sppa} = 9.9 W/cm^2, DC = 50%, SD = 300 ms) and found peak latencies of ~6.5s in monkey areas 1/2 and 3a/b. In our hands, the HRF is more similar to the responses observed by Kim et al. (2017) for mice stimulated with an extended 10 pulse trains over 5 s for each trial (f = 425 kHz, I_{sppa} = 1.84 W/cm^2, SD = 200 ms, DC = 7%, PRF = 375, 750 and 1500Hz), where the CBF changes reached a maximum value after 2.7s. Interestingly, a similar observation of a relatively rapid hemodynamic response function was also reported in Murine cortical responses to optogenetic stimulation (Kahn et al., 2013), suggesting that induced mouse cortical hemodynamic responses are generally relatively rapid.

It is also important to discuss the mechanism of cortical hemodynamic response induced by TUS. Because brain hemodynamics are regulated by neurons (Attwell et al., 2010; Sheth et al., 2005), hemodynamic changes offer an indirect way of recording brain activity based on the neurovascular coupling mechanism (Cauli and Hamel, 2010; Donahue et al., 2009). In neurovascular coupling studies, sensory stimulation is commonly used as input and the hemodynamic signal is used as the surrogate marker to readout the changes in neural activity (Galeffi et al., 2015). Earlier studies demonstrated that transcranial magnetic stimulation (Orosz et al., 2012), transcranial direct current stimulation (Paquette et al., 2011), and optogenetic stimulation (Atry et al., 2015), all modulate neuronal activity simultaneously with hemodynamic changes, and our study adds to a body of observations of TUS-induced hemodynamic changes putatively mediated via neurovascular coupling. Moreover, in our detailed observations of the amplitudes of variable neural-vascular-motor responses to repeated TUS stimulations, we found a strong linear coupling relationship between the CBF, LFP and EMG responses to a large ensemble of repeated stimuli. In particular, Fig. 4(C) shows a large 'dynamical range' of varying LFP responses appears to be strongly correlated with a similarly large range of CBF responses, consistent with a scenario where the CBF response is 'driven' by the neural responses.

Hemodynamics are a crucial component of brain function (Dunn et al., 2005), motivating the detailed study of the hemodynamic responses to different ultrasonic parameters in this study. Our results demonstrate a systematic relationship between the CBF and UI, SD and DC parameters, which was previously only accomplished for behavioral motor output (King et al., 2013), rather than brain activity-related measures. CBF peak values increased with increasing I_{sppa} and SD, even for a non-saturating intensity level (0.8 W/cm^2). The weak dependence on duty cycle is not predicted by this model (Kim et al., 2014; Plaksin et al., 2014), and definitely merits further scrutiny and study. Our study can provide a reference for the choice of parameters for future TUS experiments, including response mapping studies, similar to those performed using optogenetics (Bauer et al., 2018). Interestingly, Li et al. found that rats with LIPUS had smaller ischemic areas during stroke induction (Li et al., 2017). They used low-intensity ultrasound to protect ischemic brain injury and observed significant increase of CBF after TUS, which could be neuroprotective in ischemic brain injury. Our results, which demonstrate the relationship between the CBF and ultrasonic parameters, can perhaps be used as a reference for the choice of parameters for TUS in the application of brain protection during ischemic stroke.

Recently, Guo et al. (2018) and Sato et al. (2018) reported that ultrasound stimulation activates cortical neurons by non-specific auditory responses. However, these results are countered in a recent report by Mohammadjavadi et al. (2019), who used low-intensity ultrasound to stimulate wild-type normal hearing mice and genetically deaf mice and simultaneously recorded the EMG signals to monitor the motor response induced by ultrasound. Mohammadjavadi et al. (2019) found that the motor responses of two different strains of deaf knockout mice are the same as in normal hearing wild type mice, demonstrating that direct activation of central motor neural circuits is via ultrasound stimulation rather than via a startle reflex by auditory responses. Furthermore, Mohammadjavadi et al. (2019) present compelling arguments for a relatively weak auditory response expected in mice for a 1 kHz-modulated waveform, as we have used here. In the context of this ongoing controversy, we believe that our study putatively presents directly ultrasound-mediated hemodynamic responses, however, future research is needed to further clarify which component of these responses may be mediated by off-target effects.

5. Conclusion

In summary, we used electrophysiological recording and high temporal resolution laser speckle contrast imaging for real-time monitoring of motor response, neural activity and cortical hemodynamic responses modulated by a single short pulse TUS. Our results clearly indicate that short, low-intensity TUS pulses induce immediate motor response and neural activity, and rapid hemodynamic response selectively at the stimulation site. We also demonstrate a linear coupling relationship between CBF, LFP and EMG amplitudes. Multi-parameter TUS experiments demonstrate that the CBF monotonically increases for increasing ultrasonic intensity and stimulus duration. These results will inform and enable future studies of global hemodynamic responses to TUS in both animal and human brains, using modalities such as functional MRI, ultrasound or opto-acoustic imaging, where statistical analysis is typically guided by a stereotypical hemodynamic response function.

Declaration of competing interest

The author(s) declare no potential conflicts of interest with respect to the research, authorship, and/or publication of this article.

CRediT authorship contribution statement

Yi Yuan: Conceptualization, Methodology, Software, Writing - original draft. **Zhijie Wang:** Data curation, Methodology, Software, Writing - original draft. **Mengyang Liu:** Software, Writing - original draft. **Shy Shoham:** Supervision, Conceptualization, Writing - review & editing.

Data and code availability statement

The data and code that support the findings of this study are available from the corresponding authors, upon reasonable request.

Declaration of competing interest

The author(s) declare no potential conflicts of interest with respect to the research, authorship, and/or publication of this article.

Acknowledgments

We thank Dr. Justin Little for his comments on the manuscript. This research was supported by Key Project of Natural Science Foundation of Hebei Province (F2018203256), Fund for Scientific Instruments of the National Natural Science Foundation of China (61827811). SS and YY are supported by NIH R01NS109885.

Appendix A. Supplementary data

Supplementary data to this article can be found online at https://doi.org/10.1016/j.neuroimage.2020.116597.

References

Atry, F., Frye, S., Richner, T.J., Brodnick, S.K., Soehartono, A., Williams, J., Pashaie, R., 2015. Monitoring cerebral hemodynamics following optogenetic stimulation via optical coherence tomography. IEEE (Inst. Electr. Electron. Eng.) Trans. Biomed. Eng. 62, 766–773.

Attwell, D., Buchan, A.M., Charpak, S., Lauritzen, M., Macvicar, B.A., Newman, E.A., 2010. Glial and neuronal control of brain blood flow. Nature 468, 232–243.

Baudewig, J., Nitsche, M.A., Paulus, W., Frahm, J., 2001. Regional modulation of BOLD MRI responses to human motor activation by transcranial direct current stimulation. Magn. Reson. Med. 45, 196–201.

Bauer, A.Q., Kraft, A.W., Baxter, G.A., Wright, P.W., Reisman, M.D., Bice, A.R., Park, J.J., Bruchas, M.R., Snyder, A.Z., Lee, J., Culver, J.P., 2018. Effective connectivity measured using optogenetically evoked hemodynamic signals exhibits topography distinct from resting state functional connectivity in the mouse. Cerebr. Cortex 28, 370–386.

Cauli, B., Hamel, E., 2010. Revisiting the role of neurons in neurovascular coupling. Front. Neuroenergetics 2, 9.

Constans, C., Mateo, P., Tanter, M., Aubry, J.F., 2018. Potential impact of thermal effects during ultrasonic neurostimulation: retrospective numerical estimation of temperature elevation in seven rodent setups. Phys. Med. Biol. 63, 025003.

Donahue, M.J., Stevens, R.D., De Boorder, M.J., Pekar, J.J., Hendrikse, J., Van Zijl, P.C., 2009. Hemodynamic changes after visual stimulation and breath holding provide evidence for an uncoupling of cerebral blood flow and volume from oxygen metabolism. J. Cerebr. Blood Flow Metabol. 29, 176–185.

Dunn, A.K., Devor, A., Dale, A.M., Boas, D.A., 2005. Spatial extent of oxygen metabolism and hemodynamic changes during functional activation of the rat somatosensory cortex. Neuroimage 27, 279–290.

Galeffi, F., Degan, S., Britz, G., Turner, D.A., 2015. Dysregulation of oxygen hemodynamic responses to synaptic train stimulation in a rat hippocampal model of subarachnoid hemorrhage. J. Cerebr. Blood Flow Metabol. 36, 696–701.

Guo, H., Mark Hamilton, I.I., Offutt, S.J., Gloeckner, C.D., Li, T., Kim, Y., Legon, W., Alford, J.K., Lim, H.H., 2018. Ultrasound produces extensive brain activation via a cochlear pathway. Neuron 98, 1020–1030.

Hubl, D., Nyffeler, T., Wurtz, P., Chaves, S., Pflugshaupt, T., Lüthi, M., Von Wartburg, R., Wiest, R., Dierks, T., Strik, W.K., Hess, C.W., Müri, R.M., 2008. Time course of blood oxygenation level-dependent signal response after theta burst transcranial magnetic stimulation of the frontal eye field. Neuroscience 151, 921–928.

Hynynen, K., Vykhodtseva, N.I., Chung, A.H., Sorrentino, V., Colucci, V., Jolesz, F.A., 1997. Thermal effects of focused ultrasound on the brain: determination with MR imaging. Radiology 204, 247–253.

Kahn, I., Knoblich, U., Desai, M., Bernstein, J., Graybiel, A.M., Boyden, E.S., Buckner, R.L., Moore, C.I., 2013. Optogenetic drive of neocortical pyramidal neurons generates fMRI signals that are correlated with spiking activity. Brain Res. 1511, 33–45.

Kim, H., Chiu, A., Lee, S.D., Fischer, K., Yoo, S.S., 2014. Focused ultrasound-mediated non-invasive brain stimulation: examination of sonication parameters. Brain Stimul. 7, 748–756.

Kim, E., Anguluan, E., Kim, J.G., 2017. Monitoring cerebral hemodynamic change during transcranial ultrasound stimulation using optical intrinsic signal imaging. Sci. Rep. 7, 13148.

King, R.L., Brown, J.R., Newsome, W.T., Pauly, K.B., 2013. Effective parameters for ultrasound-induced in vivo neurostimulation. Ultrasound Med. Biol. 39, 312–331.

Koch, S.P., Werner, P., Steinbrink, J., Fries, P., Obrig, H., 2009. Stimulus-induced and state-dependent sustained gamma activity is tightly coupled to the hemodynamic response in humans. J. Neurosci. 29, 13962–13970.

Lee, W., Kim, H., Jung, Y., Song, I.U., Chung, Y.A., Yoo, S.S., 2015. Image-guided transcranial focused ultrasound stimulates human primary somatosensory cortex. Sci. Rep. 5, 8743.

Li, N., Jia, X., Murari, K., Parlapalli, R., Rege, A., Thakor, N.V., 2009. High spatiotemporal resolution imaging of the neurovascular response to electrical stimulation of rat peripheral trigeminal nerve as revealed by in vivo temporal laser speckle contrast. J. Neurosci. Methods 176, 230–236.

Li, H., Sun, J., Zhang, D., Omire-Mayor, D., Tong, S., 2017. Low-intensity (400 mW/cm2, 500 kHz) pulsed transcranial ultrasound preconditioning may mitigate focal cerebral ischemia in rats. Brain Stimul. 10, 695–702.

Mohammadjavadi, M., Peiyong Ye, P., Xia, A., Brown, J., Popelka, G., Pauly, K.B., 2019. Elimination of peripheral auditory pathway activation does not affect motor responses from ultrasound neuromodulation. Brain Stimul. 12, 901–910.

Naor, O., Krupa, S., Shoham, S., 2016. Ultrasonic neuromodulation. J. Neural. Eng. 13, 031003.

Orosz, A., Jann, K., Wirth, M., Wiest, R., Dierks, T., Federspiel, A., 2012. Theta burst TMS increases cerebral blood flow in the primary motor cortex during motor performance as assessed by arterial spin labeling (ASL). Neuroimage 61, 599–605.

Paquette, C., Sidel, M., Radinska, B.A., Soucy, J.P., Thiel, A., 2011. Bilateral transcranial direct current stimulation modulates activation-induced regional blood flow changes during voluntary movement. J. Cerebr. Blood Flow Metabol. 31, 2086–2095.

Plaksin, M., Shoham, S., Kimmel, E., 2014. Intramembrane cavitation as a predictive bio-piezoelectric mechanism for ultrasonic brain stimulation. Phys. Rev. X 4, 011004.

Plaksin, M., Kimmel, E., Shoham, S., 2016. Cell-type-selective effects of intramembrane cavitation as a unifying theoretical framework for ultrasonic neuromodulation. Eneuro 3, 1–16.

Sato, T., Shapiro, M.G., Tsao, D.Y., 2018. Ultrasonic neuromodulation causes widespread cortical activation via an indirect auditory mechanism. Neuron 98, 1031–1041.

Sheth, S.A., Nemoto, M., Guiou, M., Walker, M., Toga, A.W., 2005. Spatiotemporal evolution of functional hemodynamic changes and their relationship to neuronal activity. J. Cerebr. Blood Flow Metabol. 25, 830–841.

Shih, Y.Y.I., Yash, T.V., Rogers, B., Duong, T.Q., 2014. fMRI of deep brain stimulation at the rat ventral posteromedial thalamus. Brain Stimul. 7, 190–193.

Thomson, R.H., Maller, J.J., Daskalakis, Z.J., Fitzgerald, P.B., 2011. Blood oxygenation changes resulting from suprathreshold transcranial magnetic stimulation. Brain Stimul. 4, 165–168.

Tufail, Y., Yoshihiro, A., Pati, S., Li, M.M., Tyler, W.J., 2011. Ultrasonic neuromodulation by brain stimulation with transcranial ultrasound. Nat. Protoc. 6, 1453–1470.

Vykhodtseva, N., Sorrentino, V., Jolesz, F.A., Bronson, R.T., Hynynen, K., 2000. MRI detection of the thermal effects of focused ultrasound on the brain. Ultrasound Med. Biol. 26, 871–880.

Yang, P., Phipps, M.A., Newton, A.T., Chaplin, V., Gore, J.C., Caskey, C.F., Chen, L.M., 2018. Neuromodulation of sensory networks in monkey brain by focused ultrasound with MRI guidance and detection. Sci. Rep. 8, 7993.

Yoo, S.S., Bystritsky, A., Lee, J.H., Zhang, Y., Fischer, K., Min, B.K., McDannold, N.J., Pascual-Leone, A., Jolesz, F.A., 2011. Focused ultrasound modulates region-specific brain activity. Neuroimage 56, 1267–1275.

Younan, Y., Deffieux, T., Larrat, B., Fink, M., Tanter, M., Aubry, J.F., 2013. Influence of the pressure field distribution in transcranial ultrasonic neurostimulation. Med. Phys. 40, 082902.
Yu, K., Sohrabpour, A., He, B., 2016. Electrophysiological source imaging of brain networks perturbed by low-intensity transcranial focused ultrasound. IEEE (Inst. Electr. Electron. Eng.) Trans. Biomed. Eng. 63, 1787–1794.
Yuan, Y., Yan, J.Q., Ma, Z.T., Li, X.L., 2016. Effect of noninvasive focused ultrasound stimulation on gamma oscillations in rat hippocampus. Neuroreport 27, 508–515.
Yuan, Y., Wang, Z.J., Wang, X.R., Yan, J.Q., Liu, M.Y., Li, X.L., 2019. Low-intensity pulsed ultrasound stimulation induces coupling between ripple neural activity and hemodynamics in the mouse visual cortex. Cerebr. Cortex 29, 3220–3223.